JMB

Dynamic Structure of Retinylidene Ligand of Rhodopsin Probed by Molecular Simulations

Pick-Wei Lau[1], Alan Grossfield[2], Scott E. Feller[3] Michael C. Pitman[2] and Michael F. Brown[1,4,5]*

[1]*Department of Biochemistry and Molecular Biophysics University of Arizona Tucson, AZ 85721, USA*

[2]*IBM TJ Watson Research Center, Yorktown Heights NY 10598, USA*

[3]*Department of Chemistry Wabash College, Crawfordsville IN 47933, USA*

[4]*Department of Chemistry University of Arizona Tucson, AZ 85721, USA*

[5]*Department of Physics University of Arizona Tucson, AZ 85721, USA*

Rhodopsin is currently the only available atomic-resolution template for understanding biological functions of the G protein-coupled receptor (GPCR) family. The structural basis for the phenomenal dark state stability of 11-*cis*-retinal bound to rhodopsin and its ultrafast photoreaction are active topics of research. In particular, the β-ionone ring of the retinylidene inverse agonist is crucial for the activation mechanism. We analyzed a total of 23 independent, 100 ns all-atom molecular dynamics simulations of rhodopsin embedded in a lipid bilayer in the microcanonical (*N,V,E*) ensemble. Analysis of intramolecular fluctuations predicts hydrogen-out-of-plane (HOOP) wagging modes of retinal consistent with those found in Raman vibrational spectroscopy. We show that sampling and ergodicity of the ensemble of simulations are crucial for determining the distribution of conformers of retinal bound to rhodopsin. The polyene chain is rigidly locked into a single, twisted conformation, consistent with the function of retinal as an inverse agonist in the dark state. Most surprisingly, the β-ionone ring is mobile within its binding pocket; interactions are non-specific and the cavity is sufficiently large to enable structural heterogeneity. We find that retinal occupies two distinct conformations in the dark state, contrary to most previous assumptions. The β-ionone ring can rotate relative to the polyene chain, thereby populating both positively and negatively twisted 6-s-*cis* enantiomers. This result, while unexpected, strongly agrees with experimental solid-state ^{2}H NMR spectra. Correlation analysis identifies the residues most critical to controlling mobility of retinal; we find that Trp265 moves away from the ionone ring prior to any conformational transition. Our findings reinforce how molecular dynamics simulations can challenge conventional assumptions for interpreting experimental data, especially where existing models neglect conformational fluctuations.

© 2007 Elsevier Ltd. All rights reserved.

Keywords: G protein-coupled receptor; molecular dynamics; retinal; rhodopsin; vision

*Corresponding author

Present address: P.-W. Lau, Department of Molecular Biology, The Scripps Research Institute, La Jolla, CA 92037, USA.

E-mail address of the corresponding author: mfbrown@u.arizona.edu

Introduction

G-protein coupled receptors (GPCRs) constitute the largest superfamily of proteins in the human genome, and they initiate many signal transduction pathways.[1–3] This class of proteins is of enormous pharmaceutical interest,[4,5] because over 50% of recently launched drugs are targeted to GPCRs with annual worldwide sales exceeding $30 billion.[6] As with many membrane proteins it is typically quite difficult to express and characterize GPCRs. The exception is rhodopsin, the primary dim light receptor, which is the only GPCR whose atomic-level structure has been published.[7–10] A great deal

of effort has been put into developing our understanding of rhodopsin function,[11–20] both for its own sake and as a template to explain activation of other GPCRs.[3] Here we address the general problem of protein–ligand interactions in GPCRs in relation to their agonist and inverse agonist or antagonist roles. Specifically, we investigated the basis for the phenomenal dark state stability and activation of 11-*cis* retinal bound to rhodopsin at the single molecule level using an ensemble of molecular dynamics (MD) simulations. Our findings yield a deeper understanding of the structural basis for dark state retinal bound to rhodopsin, with potential insights into GPCR activation in general.[3]

The light-absorbing moiety 11-*cis* retinal of rhodopsin is bound by a protonated Schiff base linkage to the side-chain of Lys296. In its 11-*cis* conformation, retinal functions as a strong inverse agonist,[21] virtually locking the protein in the inactive state. Remarkably, upon absorbing a photon it instantly isomerizes (within 200 fs)[17,22] to the all-*trans* state, and subsequently becomes an agonist.[13,14] The protein relaxes through a series of spectroscopically defined intermediates[23] until it reaches the metarhodopsin I (MI) state, which exists in equilibrium with the active metarhodopsin II (MII) state.[13,14,16,18] The central role of retinal in directing this relaxation and promoting MII formation has been extensively investigated by a number of approaches. Studies of rhodopsin regenerated with chemically modified retinals as well as rhodopsin mutants show that specific interactions between retinal and the binding pocket of the receptor are implicated both in rhodopsin pigment formation and receptor activation.[13,16,24] Most of the altered ligands are less effective agonists in the all-*trans* state, shifting the MI–MII equilibrium back toward MI.[25–27] The C9-methyl group distal to the retinylidene Schiff base of Lys296 is known to play an essential role.[25,27,28] Moreover, the β-ionone ring of retinal is crucially important for rhodopsin activation.[26,29,30] While the flexibility of dark state retinal has not been addressed specifically in the literature, some studies have postulated that the β-ionone ring is the more dynamic region of the retinal molecule.[31] For example, ^{2}H NMR results have been published suggesting both a 6-s-*trans*[32] and 6-s-*cis*[33] conformation. Recent experiments, including a 2.2 Å crystal structure of rhodopsin[9] and solid state ^{13}C NMR measurements,[31] suggest the β-ionone ring is in a negatively twisted 6-s-*cis* conformation. Nonetheless, there is some ambiguity in interpreting these results, since in the crystal structure retinal has severe steric clashes, while the ^{13}C NMR experiments cannot differentiate between negatively and positively twisted enantiomers.

In addition to experimental studies, computational approaches, including molecular mechanics and quantum mechanical calculations, have been applied to understand the behavior of rhodopsin.[34–37] Although several calculations have focused on the structure of the retinal,[38] none considered the possibility of multiple retinal conformers. In part, this is because such transitions occur very rarely on the time scale of typical molecular dynamics calculations. Here we show that by utilizing an ensemble of MD simulations, we are able to relate the temporal dynamics of retinal in dark state rhodopsin to solid-state ^{2}H NMR and resonance Raman data.[17,33] By conducting multiple MD simulations, with independent starting membrane configurations, we more effectively sample the conformational space of the retinylidene ligand of rhodopsin. The results of individual simulations differ significantly, indicating they are not long enough to be compared directly to experimental results on an individual basis. Yet when taken as an ensemble, the simulations produce theoretical ^{2}H NMR spectra in excellent agreement with the experiment.[33] The data clearly show that retinal undergoes fluctuations on timescales comparable to the simulation trajectories. A model including multiple retinal conformations in the dark state is most consistent with experimental measurements. The picture that emerges suggests specific interactions with the polyene chain and the protonated Schiff base; but more surprisingly, non-specific interactions with the ionone ring allow the binding pocket to accommodate conformational heterogeneity that may optimize receptor activation.

Results

A total of 23 independently equilibrated MD simulations of 100 ns duration were carried out for a single rhodopsin molecule embedded in a fully hydrated bilayer of native-like phospholipids comprising 1-stearoyl-2-docosahexaenoyl-*sn*-glycero-3-phosphoethanolamine (SDPE)/ 1-stearoyl-2-docosahexaenoyl-*sn*-glycero-3-phosphocholine (SDPC)/ cholesterol (50:49:24). Simulations were conducted in the microcanonical (*N,V,E*) ensemble using the atomic-level structure of rhodopsin (PDB code 1U19)[9] shown in Figure 1(a). The 11-*cis* retinal chromophore of rhodopsin is bound through a protonated Schiff base linkage to Lys296, cf. Figure 1(b). Gas phase quantum chemical[39] and molecular mechanics calculations indicate three stable rotamers for the C6–C7 torsion angle which defines the orientation of the β-ionone ring relative to the polyene backbone. These include a skewed 6-s-*trans* conformation ($\chi \approx 160°$), a negatively twisted 6-s-*cis* conformer ($\chi \approx -60°$), and a positively twisted 6-s-*cis* conformer ($\chi \approx 55°$). The most recent crystal structure of rhodopsin[9] reports a C6–C7 torsion angle of $-34°$, quite far from any minima in the potential energy surface. However, interpreting this structure is problematic at best because of steric clashes between the C8 and C5-methyl (C18) hydrogen atoms. The discrepancy could in part be due to the fact that crystallography averages away thermal motion to produce only a single structure. By contrast, MD simulations directly reveal conformational heterogeneity that would be hidden experimentally. We were able to interpret experimental results, including hydrogen-out-of-plane (HOOP) wagging modes
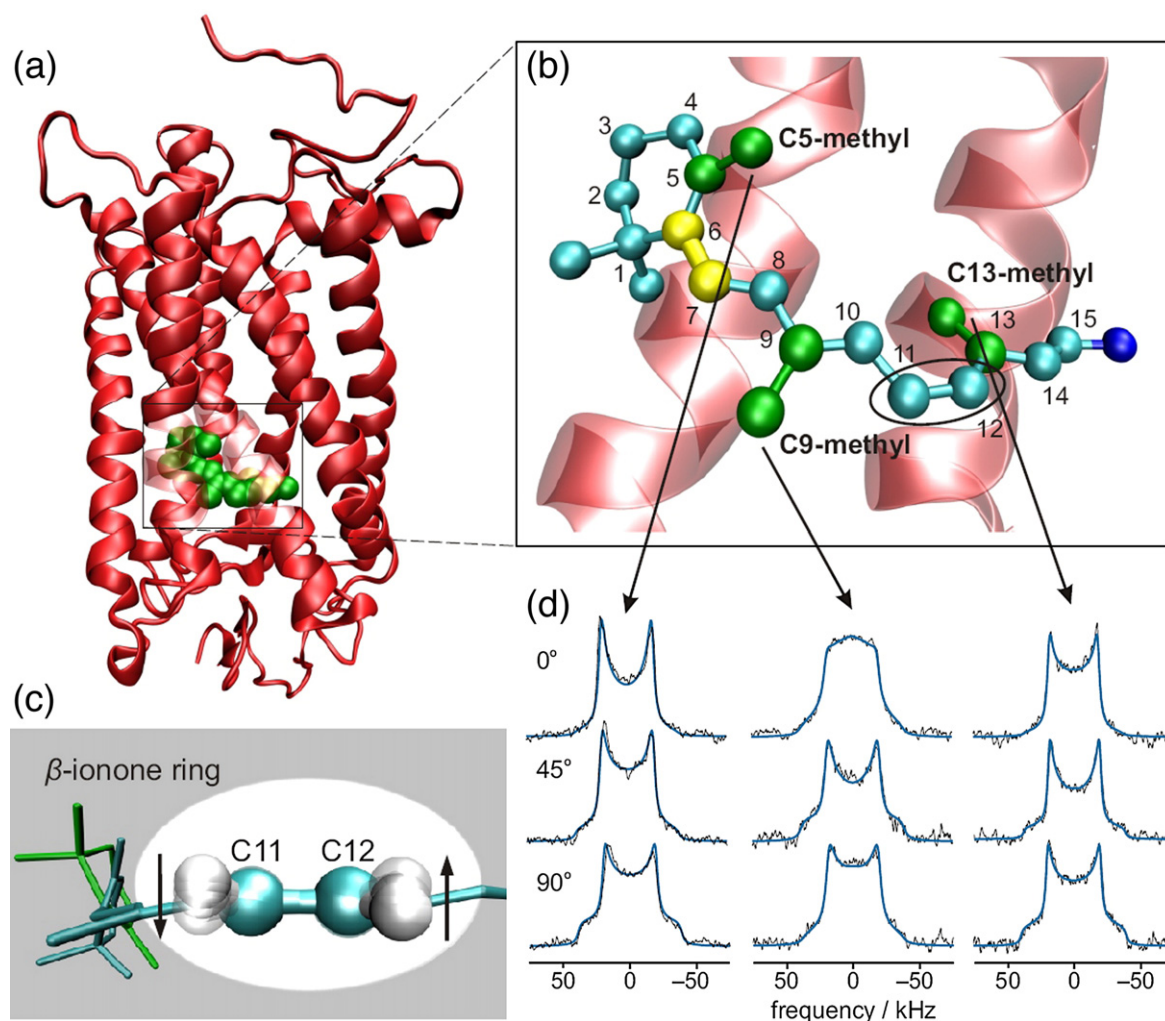
Figure 1. Structure of dark-state rhodopsin and retinal in its binding cavity is illuminated by X-ray crystallography, resonance Raman, and solid-state ^{2}H NMR spectroscopy. (a) Structural model of rhodopsin (PDB code 1U19)[9] showing retinal (green) within its binding pocket. (b) Extended view of the retinal binding pocket showing the C6–C7 bond (yellow) and the key C5, C9, and C13-methyl groups. (c) HOOP modes for H11 and H12[17] are identified at 910 cm^{-1} and are independent of both negative (cyan) and positive (green) 6-s-*cis* conformers. (d) Comparison of experimental solid-state ^{2}H NMR spectra[33] to theoretical spectra for C5, C9, and C13-methyl groups with membrane tilt angles of 0, 45, and 90° and bond orientation distributions from MD simulations.

from Raman vibrational spectroscopy[17] and solid state ^{2}H NMR spectra[33] (cf. Figure 1(c)–(d)) in terms of multiple conformers of the retinal ligand bound to rhodopsin. Comparison was made to detailed experimental data in all cases.[17,33,40,41]

Hydrogen-out-of-plane wagging modes are identified in simulations

Unlike NMR and X-ray methods, Raman spectroscopy probes the fluctuations arising from molecular vibrations. These fluctuations are extremely sensitive to conformational changes in retinal, and can serve as an indicator of the different photointermediates.[42] In dark-state rhodopsin, a peak at 969 cm^{-1} is assigned to concerted HOOP wagging motions of the C11 and C12 hydrogen atoms.[17] Upon photoactivation, the frequency of this mode shifts significantly. When we characterized the retinal fluctuations in our simulations using princi-

pal component analysis, we observed an analogous vibrational mode with a frequency of 910 cm^{-1} that is depicted in Figure 1(c) (see Methods for details). Given the difficulties in reproducing vibrational spectra using classical molecular mechanics force fields, a 10% discrepancy between simulation and experiment is impressive. We performed this calculation separately for retinals in both the negatively and positively twisted conformations, and found that they produced similar modes at the same frequency, suggesting that this vibrational mode is independent of the conformation of β-ionone ring. As a result, the Raman experiments do not differentiate between the two conformations.

Multiple β-ionone ring conformations are consistent with ^{2}H NMR data

In solid state NMR spectroscopy, molecular interactions are measured through angular and dis-

tance restraints, giving both structure and dynamics. Salgado *et al.*[33] reported ^{2}H NMR spectra of aligned recombinant membranes containing rhodopsin regenerated with retinal deuterated at the C5, C9, or C13-methyl positions. By varying the membrane tilt angle with respect to the magnetic field, they obtained detailed information about the orientation θ_B for the individual retinylidene C–C^{2}H$_3$ bonds. Data were analyzed by assuming a single orientation for each methyl group. In the present work, we adopted a different strategy and used the simulation results to predict the ^{2}H NMR spectra. We did this by using the probability distribution from the MD simulations to compile a weighted-average spectrum in terms of theoretical spectra for each bond orientation.[43] The results are shown in Figure 1(d). The C5–C^{2}H$_3$ bond axis distribution is particularly important, because changes in the C6–C7 torsion angle report on the β-ionone ring conformation. As shown in Figure 1(d), the spectrum computed from the simulation matches the experiment extremely well. Interestingly, the probability distribution contains significant contributions from distinct conformations whose ^{2}H NMR spectra differ greatly from experiment (see below). The simulated spectra are most similar to experiment when computed from the probability distribution derived directly from the combined MD simulations. For completeness, we performed the same analysis for the C9 and C13-methyl groups, as also shown in Figure 1(d), where the simulations predict a single dominant conformer consistent with the crystal structure. The fact that the spectra agree well in all cases lends support to the idea that the β-ionone ring has more than one conformation in the dark-state rhodopsin binding pocket.

Flexibility of retinal ligand is illuminated by large-scale simulations

Turning next to the issue of the β-ionone ring conformation, Figure 2(a) shows the distribution of the C6–C7 torsion angles compiled from all 23 simulations. Two 6-s-*cis* conformers are populated, with the negatively twisted ($\chi \approx -60°$) conformer predominating, but with a significant probability for the positively twisted ($\chi \approx +70°$) conformation. Gas phase computations indicate equal probability for the two 6-s-*cis* conformers, suggesting that the asymmetry in the distribution for the β-ionone ring of retinal when bound to rhodopsin is most likely due to interactions with the surrounding protein side-chains. Previous experiments using chemically modified ligands have demonstrated that the binding cavity differentiates between retinal enantiomers.[16,40] Our MD simulations imply that the cavity has a moderate selectivity for the negatively twisted enantiomer, yielding positive ellipticity in circular dichroism (CD) spectra consistent with experimental data.[40]

The conformation of the β-ionone ring has also been investigated through measurements of the C8-to-C18 distance using solid-state rotational resonance ^{13}C NMR spectroscopy.[31] In Figure 2(b) the
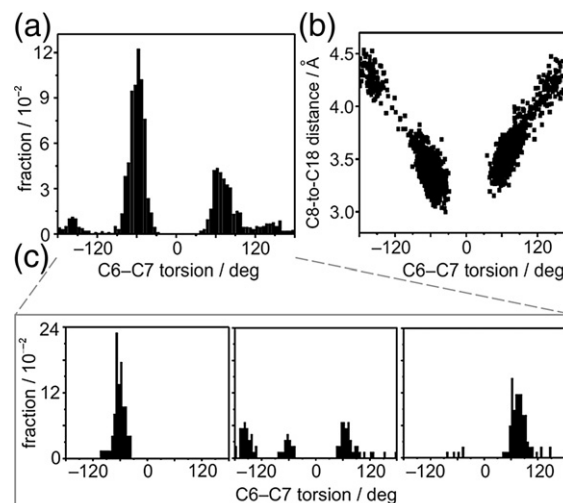

Figure 2. Multiple conformations of the β-ionone ring of the retinylidene inverse agonist are shown by molecular simulations. (a) Distribution of the C6–C7 torsion angle in all 23 simulations of 100 ns duration. The two most prevalent conformations are shown, representing negatively and positively twisted 6-s-*cis* conformations of the β-ionone ring. (b) Plot of C8-to-C18 internuclear distance as a function of C6–C7 torsion angle showing the symmetry with respect to 0°. (c) Three representative C6–C7 torsion angle distributions from the 23 individual 100 ns trajectories comprising the distribution in (a).

probability distribution for the C8-to-C18 carbon distance is plotted as a function of the C6–C7 torsion angle obtained in the simulations. Figure 2(b) clearly demonstrates that the distance is correlated with the β-ionone ring orientation; it also shows that the distance is governed solely by the magnitude of the 6-s-*cis* skew and not the sign, due to the mirror image symmetry of the two enantiomers. As a direct result, the rotational resonance experiment cannot distinguish between the positively and negatively twisted conformers. Moreover, the C8-to-C18 distance varies over a large range, from approximately 3.0 Å to 4.5 Å, with the smaller distances corresponding to a conformation in the 6-s-*cis* region, and the larger distances representing the 6-s-*trans* region. For a particular value of the C6–C7 torsion, there are substantial variations in the observed C8-to-C18 internuclear distances, arising from fluctuations in bond angles and bond lengths. This is important when using the distance from NMR as a restraint for the conformation of retinal, because the distance for a single conformer will in general differ from that computed by averaging over the conformational fluctuations. Figure 2(c) shows representative C6–C7 torsion angle distributions from individual simulations, which are further discussed below.

We now shift our focus to the conformation of the polyene moiety of the retinylidene chromophore within the binding cavity of the photoreceptor, showing in Figure 3 the probability distributions for the torsion angles along the entire conjugated chain. In contrast to the C6–C7 dihedral angle, the torsions in the polyene chain all have narrow unimodal
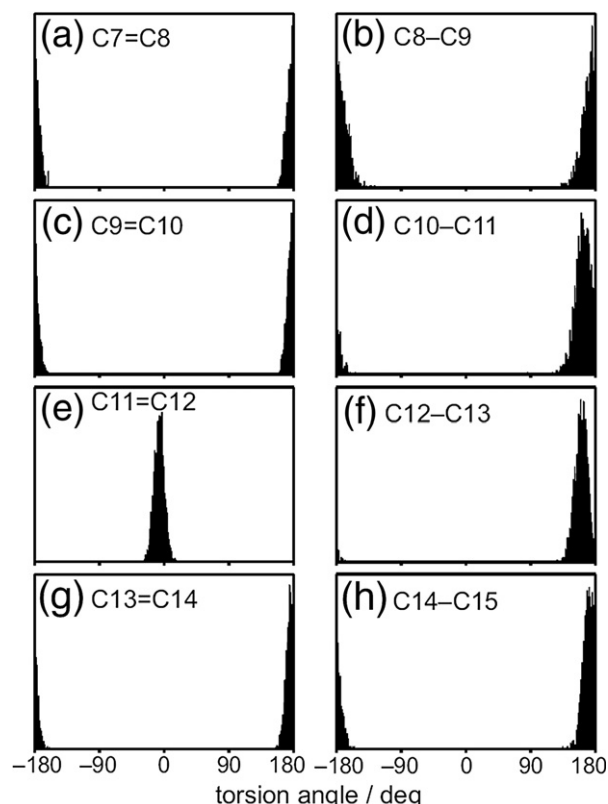
Figure 3. The polyene chain of retinylidene ligand is locked in a twisted conformation in the inverse agonist form. (a)–(h) Torsion angle distributions along the conjugated polyene chain from C7 to C15. Twisting of the polyene chain from planarity (torsion angle $\chi = 180°$) is mainly confined to the C10–C11 and C12–C13 torsions to either side of the C11=C12 double bond.

distributions, indicating that it exists in a single well-defined state. All the torsion angles (C7 to C15) are in the *trans* conformation, except the C11=C12 bond which is in the *cis* conformation. Any concerted deviation from planarity is an indication of strain induced by the protein environment, and may strongly alter the photochemistry of the polyene chain. For retinal bound to rhodopsin, the two torsions adjacent to the *cis*-double bond are significantly perturbed from their planar state; the C10–C11 torsion angle is 164(±12)° and the C12–C13 torsion angle is 161(±9)°, in accord with ^{2}H NMR data for rhodopsin in the dark state.[33] The torsional deformation alleviates the steric clashes between the C13-methyl group and the H10 hydrogen.[38] Results of the MD simulations are generally consistent with three planes of unsaturation for retinal within the binding cavity of rhodopsin,[16,33,41] a model previously used to interpret ^{2}H NMR results.[33]

Sampling and ergodicity are established through multiple trajectories

Although the polyene chain of the retinylidene chromophore occupies a single well-defined conformation, the ensemble of MD simulations reveals

that the β-ionone ring populates two distinct enantiomers (cf. Figure 2(a)). Previous MD and quantum mechanics/molecular mechanics (QM/MM) simulations did not report multiple retinal conformations,[9,34,35,44] most likely due to limitations in time scale. Based on the number of transitions in our simulations, the lifetimes of the two conformers are ≈ 50 ns, comparable to the longest of the other trajectories. Because transitions are rare events, the probability distributions for independent trajectories differ significantly, indicating that the 100 ns timescale is not long enough to allow statistical convergence. This point is best seen in Figure 2(c), which shows probability distributions from three of the 23 trajectories. These differences highlight the risks involved in interpreting a single trajectory, no matter how long, when the system may contain long-lived states. For any given trajectory, the C6–C7 torsion angle undergoes only a small number of transitions. Indeed, in several simulations the torsion remains in its initial conformation throughout the trajectory, with no transitions at all. In others, there is a single transition leading to a positively twisted conformation, and still others show a number of transitions back and forth.

As noted above, trajectories where the retinal primarily samples the positive-twisted conformation produce ^{2}H NMR spectra that bear little resemblance to the experimental ones; interpreted by themselves they would lead us to conclude that the simulations and experiments were fundamentally inconsistent. On the other hand, combining the positive 6-s-*cis* conformers with the negatively twisted state, using the ensemble of simulations to provide the weighting, improves the fit to experimental data[33] *versus* the negatively twisted state alone. It is only by interpreting the ensemble average of the simulations in accord with the ergodic hypothesis that we are able to conclude that there are multiple important conformations within the actual distribution. To illustrate this aspect further, Figure 4 shows ^{2}H NMR spectra calculated by restricting the angular range of the probability distribution from all 23 simulations. Part (a) considers only values of the C6–C7 torsion angle <0°; whereas part (b) only includes angles >0°, with the entire distribution indicated in (c). As can be seen, considering only a part of the distribution leads to very poor agreement of the synthetic spectra with the experimental ^{2}H NMR data; yet when the entire distribution is included the agreement is more gratifying (cf. Figure 1).

Contact residues of β-ionone ring depend on its conformation

To assess the change in protein environment due to isomerization about the C6–C7 bond, we mapped the interactions of the three retinal methyl carbons (C5, C9, and C13) with the neighboring protein residues. Specifically, we identified the amino acid residues found within a 4 Å sphere about each methyl carbon in each of the 23 simulations. For each simulation, we
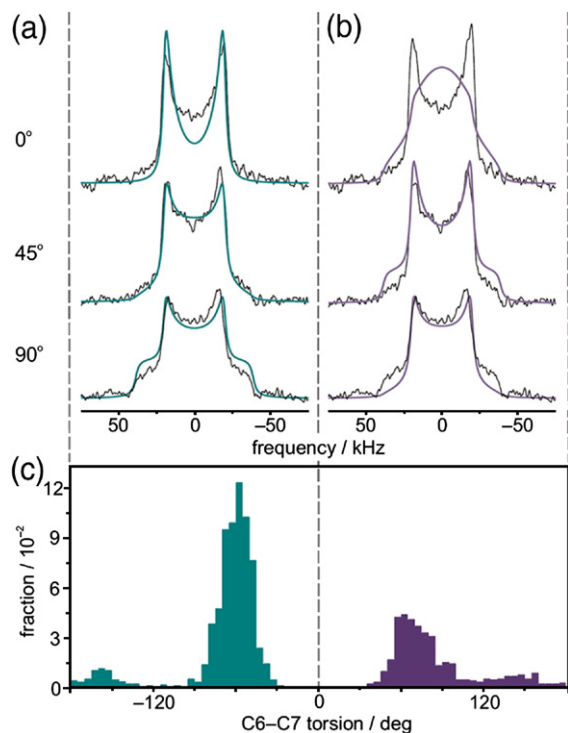
Figure 4. Retinal ligand of rhodopsin has conformations of β-ionone ring whose ^{2}H NMR spectra differ from experiment. (a) Predicted ^{2}H NMR spectra considering only distribution of C6–C7 torsion angles <0° (cyan) and (b) torsion angles >0° (purple). Synthetic spectra in each case are superimposed on experimental ^{2}H NMR data[33] for membrane tilt angles of 0, 45, and 90°. (c) Probability distribution for all 23 simulations (cf. Figure 2) showing range of C6–C7 torsional angles used to calculate the synthetic spectra.

constructed a vector containing the probability that a selected region of retinal formed a contact with each residue, and combined them to form a contact probability matrix **C**. The average contact probability for each residue was computed over all 23 simulations and subtracted from each column of the **C** matrix, producing a fluctuation matrix. The covariance matrix $\mathbf{V} = \mathbf{C}^{\mathbf{T}}\mathbf{C}$ was then constructed, where $\mathbf{C}^{\mathbf{T}}$ is the transposed contact matrix. Covariance matrices for each of the methyl groups are represented in Figure 5(a)–(c), and allow one to compare the trajectories and identify patterns in ligand–protein interaction. Figure 5(a) shows **V** for the C5-methyl group, the most mobile of the three due to its location on the β-ionone ring. This map can be divided into three different blocks, giving three characteristic distributions of the C6–C7 torsion: (i) simulations 1–11, which mostly populate the negatively twisted 6-s-*cis,* (ii) simulations 12–15, where both positively and negatively twisted states are populated, and (iii) simulations 16–23, where the positively twisted state predominates. The simulations in each group are strongly correlated with each other, and anti-correlated with those in the other groups, indicating that the torsional state directly modulates the residues which interact with the ligand. In contrast, the

covariance matrix for the C9-methyl and C13-methyl groups in Figures 5(b) and 5(c) are featureless, meaning that fluctuations of these bonds do not alter interactions of retinal with its environment.

To further enumerate the important residues in contact with the C5-methyl group, we present its contact matrix in Figure 5(d). Note that Thr118, Gly121, and Glu122 appear frequently in simulations in the first category, while residues Phe208, Tyr268, and Ala269 are often in close proximity to the C5-methyl group for simulations in the third category. Residues in contact with the C9 and C13-methyl groups are shown in Figures 5(e) and 5(f). Streaks of the same color are observed across all 23 simulations, indicating that the presence or absence of a particular residue is consistent from one simulation to another. Most striking is the close proximity of Ile189 to the C9-methyl group across all simulations. The closest residues to the C13-methyl group are Ala117, Trp265, Tyr268, Ala292, and Ala295. It follows that the polyene chain segments occupy well-defined binding sites, which may account for the phenomenal dark state stability of retinal acting as an inverse agonist. By contrast, the binding site of the β-ionone ring is not as well defined, presumably due to relatively non-selective interactions consistent with a pocket of moderate to low specificity.[16]

Trp265 inhibits 6-s-*trans* retinal formation within the binding pocket

The residue Trp265 is highly conserved across the GPCR family A, and is thought to be involved in ligand binding. Interactions between the Trp265 side-chain and the β–ionone ring in rhodopsin are implicated in the inverse agonist role of retinal.[20,24] Consistent with this interpretation, Figure 6(a) indicates that Trp265 is usually packed against retinal, specifically the ionone ring. With this in mind, we attempted to relate motions of Trp265 to conformational transitions of the retinal C6–C7 torsion angle. Examination of the probability distribution for the C6–C7 torsion, Figure 2(a), shows that the primary path between the two twisted 6-s-*cis* states is *via* the 6-s-*trans* state. Hence the *trans* state can be used as an indicator of retinal conformational transitions. By examining the time correlation function between the presence of the *trans* state and the distance between the β-ionone ring and Trp265 (Figure 6(b)), we can interpret the functional significance of these interactions. Specifically, we computed $C(t) = \langle [d(t+\tau) - \langle d \rangle] \ [\vartheta(t) - \langle \vartheta \rangle] \rangle / \sigma_d \sigma_\vartheta$ where $d(t)$ is the instantaneous distance, and $\vartheta(t)$ is an indicator function that is unity when the C6–C7 torsion is greater than 120° or less than −120°, and zero otherwise. Here $\langle d \rangle$ and $\langle \vartheta \rangle$ denote averaging over all times in all simulations, and σ_d and σ_ϑ are corresponding standard deviations.

We computed this correlation function independently for each of the 19 trajectories in which we found the *trans* state. Figure 6(b) shows the average of these correlation functions (the error bars are the
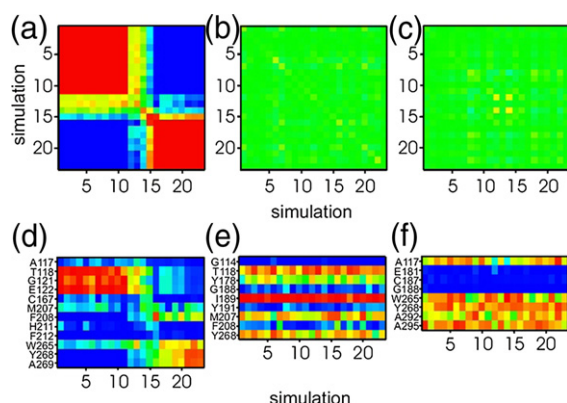
Figure 5. Covariance analysis of individual 100 ns simulations shows variability of protein environment of retinylidene C5, C9, and C13-methyl groups. Elements of the covariance matrix are depicted by colors and range from −1 (completely anti-correlated; blue) to 1 (completely correlated; red). (a)–(c) C5, C9, and C13-methyl positions, respectively. Note that the matrix in (a) has three different blocks: (i) simulations 1– 11; (ii) simulations 12– 15; and (iii) simulations 16–23. Each of the blocks has a distinct C5-methyl group environment. By contrast, in (b) and (c) the color map for the C9 and C13-methyl groups has a consistent green color, indicating all 23 simulations yield similar methyl group environments. (d)–(f) Contact matrices for the C5, C9, and C13-methyl groups, respectively. Columns list the simulation number and rows correspond to residues within a 4 Å radius sphere centered on the methyl carbon. The color scale ranges from blue (low fraction value; indicating residue is infrequent within 4 Å radius sphere) to red (high fraction value within 4 Å sphere). For each block in (a), distinct residues appear consistently around the C5-methyl group showing sampling of different environments. For the C9 and C13-methyl groups in (b) and (c), bands of similar colors across all 23 simulations evince similar environments.

standard error, computed as $\sigma/\sqrt{N}$, where σ is the standard deviation and N is the number of simulations). The correlation function has a statistically significant positive peak at $\tau = -1$ ns (the resolution of the time series used to construct the correlations), indicating that on average the formation of the *trans* state is preceded by an increase in the distance between Trp265 and the β-ionone ring. It appears that conformational transitions between the two twisted 6-s-*cis* conformers are inhibited by the presence of Trp265 in its normal configuration. To further test this idea, we ran a short simulation in which we mutated Trp265 to glycine *in silico*. In this trajectory, we saw a significant population of 6-s-*trans* retinal, in contrast to the <1% population in the primary simulations. This may have functional implications, as previous work[24] suggests that rhodopsin activation moves the β-ionone group away from Trp265 toward Ala169.

Discussion

The present work shows that all-atom MD simulations provide an important framework for

relating the temporal fluctuations of retinal to its biological activity. Upon photon absorption by rhodopsin, the retinal cofactor isomerizes to the *trans* form of the polyene, which drives non-equilibrium relaxation of the protein from the dark state toward the inactive MI state. In MI, *trans*-retinal acts as an agonist, shifting the MI-MII equilibrium toward the active MII state, which binds the G protein transducin and initiates visual perception.[13,14,16] Besides the polyene chain of retinal, the β-ionone ring in particular is crucial to the reaction mechanism[20,26,29,30,45–47] The β-ionone ring is connected with protein movements that yield receptor activation,[14,20,48–50] following release of the spring-loaded conformational switch of the polyene. The torsion about the C6–C7 bond defines the orientation of the β-ionone ring relative to the polyene chain. Free retinal has been shown with both experimental[51] and computational[39] methods to exist as multiple isomers represented by 6-s-*cis* and 6-s-*trans* states, which is consistent with CD data.[40,41,52] By contrast, the retinal conformation becomes more restricted upon binding to rhodopsin, where it functions as an inverse agonist. It is interesting that in both bacteriorhodopsin[51,53] and sensory rhodopsin,[54] retinal is 6-s-*trans*; while in dark-adapted rhodopsin it is widely thought to adopt the 6-s-*cis* conformation.[33,40,55]

Activation mechanism of the GPCR prototype rhodopsin

An understanding of why nature has selected distinct conformations of retinal for different receptors may provide additional insights into the activation mechanism of rhodopsin.[33,56] As a step in this direction, we have used MD simulations to explore protein–ligand interactions and flexibility of retinal within the binding pocket of dark state rhodopsin. Our simulations are complementary to bioorganic[16,40,41] and biophysical[17,32,33] approaches, and aid the interpretation of experimental data. Binding of retinal to opsin leads to significant rotary strength in CD spectroscopy due to twisting of the chromophore.[57] A sign reversal is evident in bathorhodopsin, followed by a diminution in the subsequent intermediates.[52] Investigations of rhodopsin with chemically modified ligands further indicate how specific interactions of retinal within its binding cavity are connected with its dark state stability, as well as activation of the receptor. Removal of the C9-methyl group appears to increase ligand flexibility in the binding pocket. The absence of HOOP modes in Fourier transform infrared (FTIR) spectra for MI indicates the C10-to-C13 region has relaxed to a more planar conformation, which only occurs in MII for natural retinal.[25] A back shifting of the MI–MII equilibrium is evident leading to reduced G protein activation.[25] Opening the retinal ionone ring in acyclic analogs similarly reduces the stability of MII relative to MI,[26,29,45] although in this case the MI state appears to differ structurally from that formed with unmodified retinal.[26] Such acyclic modifications also eliminate the MI HOOP modes, thus implicating the
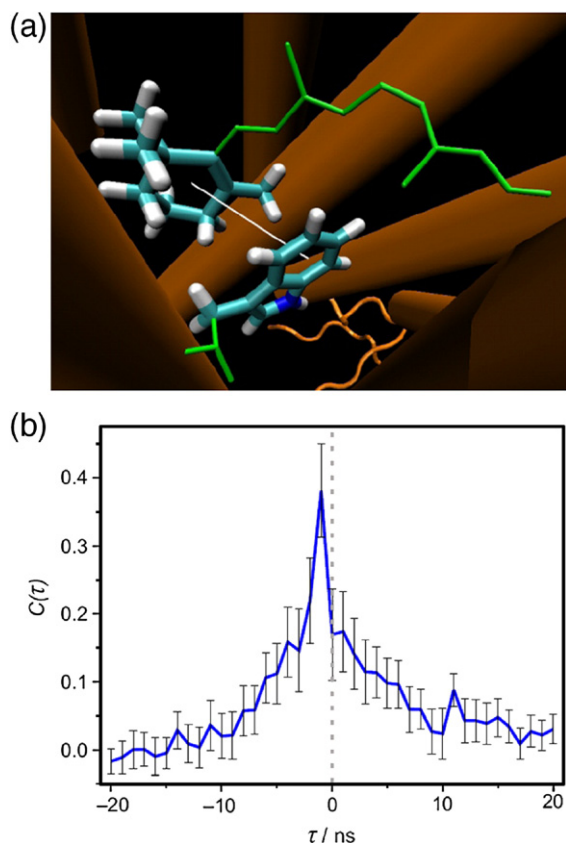
Figure 6. Conformation of the β-ionone ring is correlated with its distance to Trp265 side-chain. (a) Distance between center of the β-ionone ring and the indole 6-carbon ring of Trp265 side-chain used in the cross-correlation calculation is shown by the white line. (b) Average cross-correlation profile of the 19 simulations containing the 6-s-*trans* state shows a non-zero correlation value above the noise level at $\tau = -1$ ns. Thus a correlation between the C6–C7 torsion angle and the distance between the β-ionone ring and Trp265 is revealed.

ring structure in transmitting force from the all-*trans* retinal ligand to the protein.

The current simulations show that the polyene chain of retinal is rigidly locked into a single, twisted conformation when bound to rhodopsin, consistent with its role as an inverse agonist in the dark state. However, interactions of the β-ionone ring within its binding pocket are non-specific, and the cavity is large enough to allow conformational heterogeneity. It follows that activation of rhodopsin can be considered in terms of three (sub)sites for binding of the ligand to the receptor.[16,25,33,38] These correspond to (i) the protonated Schiff base and its associated counterion,[14,58–60] (ii) the mid-portion of the polyene chain,[25,28] and lastly (iii) the β-ionone ring within its hydrophobic binding pocket.[31,33] The three sites are specifically probed by ^{2}H NMR of the C13, C9, and C5-methyl groups, respectively.[32,33] In the dark state, the retinal polyene chain is under considerable strain, as indicated by the HOOP modes measured by stimulated Raman[17] or FTIR[26] spectroscopy, and by ^{2}H NMR of the C9 and C13-

methyl groups.[33] The HOOP modes shift their frequencies in the MI state of native rhodopsin, but disappear in MII. Likewise, solid-state ^{2}H NMR demonstrates a reduction of the twist of retinal in MI.[61] This finding suggests that the polyene strain is used to drive the large-scale protein rearrangements that occur in the MII state.[14] It is logical to consider the ring as necessary to anchor retinal to the protein, guaranteeing that retinal relaxation induces protein reorganization and gives active photoreceptor. Our work predicts that, contrary to previous assumptions, retinal populates more than one stable conformation under physiological conditions. The stron-gest evidence for the existence of multiple conformers is the excellent agreement between the experimental ^{2}H NMR spectra and those computed directly from the distribution of bond orientations observed in the MD simulations. There are additional indications of such conformational heterogeneity from rotational resonance ^{13}C NMR[31] and FTIR[62] spectroscopy.

Conformational flexibility of retinal in the inverse agonist state

Multiple retinal conformations[31] could be important for understanding conflicting reports in the literature that address isomerization of the β-ionone ring.[32–34,38,40,55,63] Up until now, most investigators have assumed that the β-ionone ring of retinal adopts a single conformer. Biophysical studies using ^{2}H NMR,[32,33] ^{13}C NMR,[64] and CD[40] spectroscopy have been interpreted in terms of only one isomer of the β-ionone ring. By contrast, MD simulations suggest that retinal may populate different conformers while bound to rhodopsin. Our results imply that the net positive ellipticity of the dark state of rhodopsin[40,41,52] originates from an enantiomeric excess of the negative isomer. The presence of symmetric conformers with both negative and positive C6–C7 torsional angles is not detectable by ^{13}C NMR studies.[31,64] As a result, previous interpretations of structural data indicating a single negatively twisted 6-s-*cis* conformation, while natural in light of the X-ray crystal structure, may be incomplete. Although the C9 and C13-methyl groups undergo only small librations, and consistently interact with the same parts of the protein, the flexibility of the C6–C7 torsion enables the C5-methyl group to interact with a more diverse set of residues. Interestingly, these internal motions do not significantly alter the overall shape of the binding pocket. Figure 7 shows the two primary retinal conformations found in this work superposed in the context of the protein cavity. Only minor local displacements of individual amino acid residues are necessary to accommodate the retinal conformational transitions. More importantly, specific interactions selecting only one of the enantiomers are apparently absent, despite the highly tuned function of rhodopsin.

Our findings highlight the importance of performing multiple MD simulations to effectively

explore conformational space with fewer assumptions and to assess convergence. In particular, the correlation between the motions of Trp265 and the retinal could not be assessed from a single trajectory; it was only by examining an ensemble with a significant number of independent transitions that the pattern became apparent. The danger of analyzing a single trajectory is that the system may be undersampled due to the limited duration, the large number of accessible states, and the relatively long lifetimes of individual conformations. The situation is exactly analogous to an issue that arises when analyzing single molecule experiments. Any single measurement may appear inconsistent with a bulk measurement, because an individual molecule may be found in states far from the mean of the population.[65,66] Consequently, the experiments must be repeated many times in order to obtain dependable statistical information, which directly parallels the computational approach taken here. We further note there are important long-timescale fluctuations of retinal so that the simulations may not necessarily be ergodic. (The ergodic hypothesis states that the time average for any one member of an ensemble is equivalent to the ensemble average at any one instant.) These statistical fluctuations are manifested as significant variations in the distribution of retinal conformers. Sampling from a number of independently equilibrated systems allows us to more closely estimate the actual molecular properties, while accurately assessing the degree of statistical convergence. However, we cannot discount the possibility that even the ensemble of simulations taken together does not represent a fully converged probability distribution for the conformation of retinal. In each simulation, the retinal was initially placed in the negatively twisted form, as suggest by the crystal structure. While this is clearly the most tenable choice, the resulting simulations may as a result overestimate the population of the negatively twisted form. Unfortunately, proving ergodicity from a finite set of data is extremely difficult, especially when the lifetime of some states is comparable to the length of the trajectories.

To conclude we propose the following mechanistic hypothesis: in the dark state, retinal acts as an inverse agonist by forming specific interactions through the polyene chain and protonated Schiff base. However, the ionone ring interactions are non-specific, and the binding pocket is large enough to allow interconversion of positively and negatively twisted 6-s-*cis* conformers. This stands in contrast to previous analyses of crystallographic and NMR data, which implicitly assume a single representative conformation for retinal, yielding (perhaps for this reason) a structure with significant internal steric clashes. Our suggestion that retinal instead populates different twisted 6-s-*cis* enantiomers enables us to resolve this difficulty. The resulting probability distribution correctly reproduces experimental ^{2}H NMR spectra, as well as resonance

Raman data. In its 11-*cis* form, retinal is a strong inverse agonist and locks the dark state into an inactive conformation that accounts for its phenomenal stability. Since modification of the ionone ring generally diminishes activity, it may seem counterintuitive that interactions between the ionone ring and the receptor are non-specific. Yet the exceptional agreement of the experimental spectra calculated from the simulation-derived conformational distributions supports multiple retinal conformers as our best model of dark state rhodopsin. Finally, the present results demonstrate that computer simulations can offer deep insights into the interpretation of experimental data, thus facilitating mechanistic models that correspondingly motivate future experiments.

Methods

Molecular dynamics simulations

System construction in the microcanonical (N,V,E) ensemble is described by Grossfield *et al.* and its Supplementary Material.[67] Briefly, each of the systems contained one rhodopsin molecule, 50 SDPE molecules, 49 SDPC molecules, 24 cholesterol molecules, 14 sodium ions, 16 chloride ions, and 7400 water molecules (43 222 atoms total). Individual systems were embedded in a 56.5 Å×79.2 Å×95.5434 Å periodic box, with the membrane normal aligned along the z-axis. The CHARMM version 27 force field was used to represent the protein[68] with parameters appropriate for retinal,[69] while the recently refined CHARMM saturated chain,[70] polyunsaturated chain,[71] and cholesterol[72] parameters were used to describe the lipids. Construction and equilibration were performed using CHARMM27,[68,73] while production calculations were performed using Blue Matter,[74] a molecular dynamics package specially written to take advantage of the Blue Gene/L hardware.[74] The simulations described here were generally run on 512, 1024, or 2048 Blue Gene nodes, generating 4, 6, or 9 ns/day, respectively. However, due to improvements in the code, we are now able to generate roughly 40 ns/day using 4 Blue Gene racks (4096 nodes). It is worth noting that this performance significantly exceeds that of the most rigorous implicit membrane models,[75,76] albeit with a dramatically larger computational investment. Each of the simulations was constructed independently; we used the 1U19 PDB file for the protein initial coordinates, and regenerated new lipid conformations from a library of structures. As a result, the distribution of lipid species and cholesterol around the protein was fully randomized at the beginning of each trajectory. The initial locations of sodium and chloride ions in the aqueous region were also determined randomly at the beginning of each simulation. Independently regenerating the membrane starting structure is crucial to effective sampling, given the microsecond timescale for lateral reorganization of the lipid bilayer. For further details see Grossfield *et al.*[67]

The vibrational modes of the retinal were computed using the quasi-harmonic analysis facility within CHARMM. We computed the time-averaged structure from the trajectory, and then obtained the atomic fluctuations in rectangular Cartesian coordinates from the
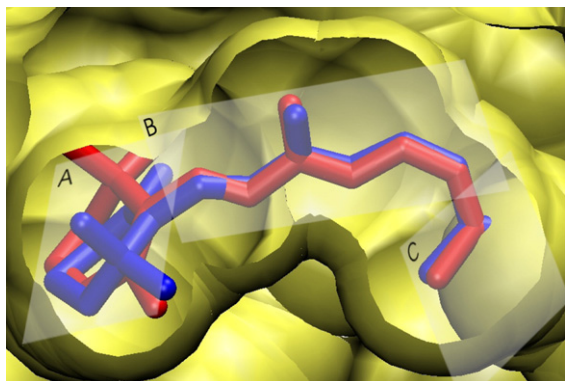
Figure 7. Dynamical structure of the retinal inverse agonist in its binding pocket is obtained for dark-state rhodopsin. Both positive (red) and negative (blue) 6-s-*cis* conformers are placed into the binding pocket of rhodopsin. The three planes used to describe the structure of retinal are designated by A, B, and C (cf. the text).

difference between the instantaneous structures and the average. The cross-correlation matrix of the fluctuations was computed and diagonalized to obtain the normal modes of the system. The normal mode associated with the HOOP motion was found by taking the scalar product of each normal mode vector with a test vector constructed by displacing H11 and H12 out of the plane of the *cis*-double bond. In each case, this procedure identified a single normal mode, whose overlap with the displacement vector was an order of magnitude greater than any other normal mode. Details of the computation of normal modes by quasi-harmonic analysis in CHARMM are described elsewhere.[77]

Calculation of ^{2}H NMR spectral lineshapes

Theoretical ^{2}H NMR lineshapes for specifically deuterated retinal bound to rhodopsin in aligned membrane bilayers were calculated as described.[33,43] Spectra were simulated for bond angles on a 1° grid; the final spectrum was then computed as the average of the individual spectra, weighted by their probability as computed from the combined molecular dynamics simulations. The mosaic spread of the membrane stack was treated as a free parameter. Further details are provided by Salgado *et al.*[33]

Acknowledgements

References

1. Bockaert, J. & Pin, J. P. (1999). Molecular tinkering of G protein-coupled receptors: an evolutionary success. *EMBO J.* **18**, 1723–1729.
2. Pierce, K. L., Premont, R. T. & Lefkowitz, R. J. (2002). Seven-transmembrane receptors. *Nature Rev. Mol. Cell Biol.* **3**, 639–650.
3. Fanelli, F. & De Benedetti, P. G. (2005). Computational modeling approaches to structure-function analysis of G protein-coupled receptors. *Chem. Rev.* **105**, 3297–3351.
4. George, S. R., O'Dowd, B. F. & Lee, S. R. (2002). G-protein-coupled receptor oligomerization and its potential for drug discovery. *Nature Rev. Drug Disc.* **1**, 808–820.
5. Watts, A. (2005). Solid-state NMR in drug design and discovery for membrane-embedded targets. *Nature Rev. Drug Disc.* **4**, 555–568.
6. Drews, J. (2000). Drug discovery: a historical perspective. *Science*, **287**, 1960–1964.
7. Palczewski, K., Kumasaka, T., Hori, T., Behnke, C. A., Motoshima, H., Fox, B. A. *et al.* (2000). Crystal structure of rhodopsin: a G protein-coupled receptor. *Science*, **289**, 739–745.
8. Okada, T., Fujiyoshi, Y., Silow, M., Navarro, J., Landau, E. M. & Shichida, Y. (2002). Functional role of internal water molecules in rhodopsin revealed by X-ray crystallography. *Proc. Natl Acad. Sci. USA*, **99**, 5982–5987.
9. Okada, T., Sugihara, M., Bondar, A.-N., Elstner, M., Entel, P. & Buss, V. (2004). The retinal conformation and its environment in rhodopsin in light of a new 2.2 Å crystal structure. *J. Mol. Biol.* **342**, 571–583.
10. Li, J., Edwards, P. C., Burghammer, M., Villa, C. & Schertler, G. F. X. (2004). Structure of bovine rhodopsin in a trigonal crystal form. *J. Mol. Biol.* **343**, 1409–1438.
11. Brown, M. F. (1994). Modulation of rhodopsin function by properties of the membrane bilayer. *Chem. Phys. Lipids*, **73**, 159–180.
12. Szundi, I., Mah, T. L., Lewis, J. W., Jäger, S., Ernst, O. P., Hofmann, K. P. *et al.* (1998). Proton transfer reactions linked to rhodopsin activation. *Biochemistry*, **37**, 14237–14244.
13. Sakmar, T. P., Menon, S. T., Marin, E. P. & Awad, E. S. (2002). Rhodopsin: insights from recent structural studies. *Annu. Rev. Biophys. Biomol. Struct.* **31**, 443–484.
14. Hubbell, W. L., Altenbach, C., Hubbell, C. M. & Khorana, H. G. (2003). Rhodopsin structure, dynamics, and activation: a perspective from crystallography, site-directed spin labeling, sulfhydryl reactivity, and disulfide cross-linking. *Adv. Protein Chem.* **63**, 243–290.
15. Botelho, A. V., Gibson, N. J., Wang, Y., Thurmond, R. L. & Brown, M. F. (2002). Conformational energetics of rhodopsin modulated by nonlamellar forming lipids. *Biochemistry*, **41**, 6354–6368.
16. Fishkin, N., Berova, N. & Nakanishi, K. (2004). Primary events in dim light vision: a chemical and spectroscopic approach toward understanding protein/chromophore interactions in rhodopsin. *Chem. Rec.* **4**, 120–135.
17. Kukura, P., McCamant, D. W., Yoon, S., Wandschneider, D. B. & Mathies, R. A. (2005). Structural observation of the primary isomerization in vision with femtosecond-stimulated Raman. *Science*, **310**, 1006–1009.

18. Palczewski, K. (2006). G protein-coupled receptor rhodopsin. *Annu. Rev. Biochem.* **75**, 743–767.

19. Botelho, A. V., Huber, T., Sakmar, T. P. & Brown, M. F. (2006). Curvature and hydrophobic forces drive oligomerization and modulate activity of rhodopsin in membranes. *Biophys. J.* **91**, 4464–4477.

20. Crocker, E., Eilers, M., Ahuja, S., Hornak, V., Hirshfeld, A., Sheves, M. *et al.* (2006). Location of Trp265 in metarhodopsin II: implications for the activation mechanism of the visual receptor rhodopsin. *J. Mol. Biol.* **357**, 163–172.

21. Han, M., Lou, J. H., Nakanishi, K., Sakmar, T. P. & Smith, S. O. (1997). Partial agonist activity of 11-*cis*-retinal in rhodopsin mutants. *J. Biol. Chem.* **272**, 23081–23085.

22. Wang, Q., Schoenlein, R. W., Peteanu, L. A., Mathies, R. A. & Shank, C. V. (1994). Vibrationally coherent photochemistry in the femtosecond primary event of vision. *Science*, **266**, 422–424.

23. Jäger, S., Lewis, J. W., Zvyaga, T. A., Szundi, I., Sakmar, T. P. & Kliger, D. S. (1997). Chromophore structural changes in rhodopsin from nanoseconds to microseconds following pigment photolysis. *Proc. Natl Acad. Sci. USA*, **94**, 8557–8562.

24. Borhan, B., Souto, M. L., Imai, H., Shichida, Y. & Nakanishi, K. (2000). Movement of retinal along the visual transduction path. *Science*, **288**, 2209–2212.

25. Vogel, R., Fan, G.-B., Sheves, M. & Siebert, F. (2000). The molecular origin of the inhibition of transducin activation in rhodopsin lacking the 9-methyl group of the retinal chromophore: a UV-Vis and FTIR spectroscopic study. *Biochemistry*, **39**, 8895–8908.

26. Vogel, R., Siebert, F., Lüdeke, S., Hirshfeld, A. & Sheves, M. (2005). Agonists and partial agonists of rhodopsin: retinals with ring modifications. *Biochemistry*, **44**, 11684–11699.

27. Vogel, R., Lüdeke, S., Siebert, F., Sakmar, T. P., Hirshfeld, A. & Sheves, M. (2006). Agonists and partial agonists of rhodopsin: retinal polyene methylation affects receptor activation. *Biochemistry*, **45**, 1640–1652.

28. Han, M., Groesbeek, M., Sakmar, T. P. & Smith, S. O. (1997). The C9 methyl group of retinal interacts with glycine-121 in rhodopsin. *Proc. Natl Acad. Sci. USA*, **94**, 13442–13447.

29. Bartl, F. J., Fritze, O., Ritter, E., Herrmann, R., Kuksa, V., Palczewski, K. *et al.* (2005). Partial agonism in a G protein-coupled receptor. Role of the retinal ring structure in rhodopsin activation. *J. Biol. Chem.* **280**, 34259–34267.

30. Domínguez, M., Álvarez, R., Pérez, M., Palczewski, K. & de Lera, A. R. (2006). The role of the 11-*cis*-retinal ring methyl substituents in visual pigment formation. *ChemBioChem.* **7**, 1815–1825.

31. Spooner, P. J. R., Sharples, J. M., Verhoeven, M. A., Lugtenberg, J., Glaubitz, C. & Watts, A. (2002). Relative orientation between the β-ionone ring and the polyene chain for the chromophore of rhodopsin in native membranes. *Biochemistry*, **41**, 7549–7555.

32. Gröbner, G., Burnett, I. J., Glaubitz, C., Choi, G., Mason, A. J. & Watts, A. (2000). Observations of light-induced structural changes of retinal within rhodopsin. *Nature*, **405**, 810–813.

33. Salgado, G. F. J., Struts, A. V., Tanaka, K., Fujioka, N., Nakanishi, K. & Brown, M. F. (2004). Deuterium NMR structure of retinal in the ground state of rhodopsin. *Biochemistry*, **43**, 12819–12828.

34. Gascon, J. A. & Batista, V. S. (2004). QM/MM study of energy storage and molecular rearrangments due to the primary event in vision. *Biophys. J.* **87**, 2931–2941.

35. Röhrig, U. F., Guidoni, L., Laio, A., Frank, I. & Rothlisberger, U. (2004). A molecular spring for vision. *J. Am. Chem. Soc.* **126**, 15328–15329.

36. Huber, T., Botelho, A. V., Beyer, K. & Brown, M. F. (2004). Membrane model for the GPCR prototype rhodopsin: hydrophobic interface and dynamical structure. *Biophys. J.* **86**, 2078–2100.

37. Lau, P.-W., Pitman, M. C., Feller, S. E. & Brown, M. F. (2005). Conformational sensitivity of retinylidene cofactor in rhodopsin studied by molecular dynamics. *Biophys. J.* **90**, 442a.

38. Sugihara, M., Hufen, J. & Buss, V. (2006). Origin and consequences of steric strain in the rhodopsin binding pocket. *Biochemistry*, **45**, 801–810.

39. Terstegen, F. & Buss, V. (1996). *Ab initio* study of the C6–C7 conformation of retinal model systems. *Chem. Letters*, **25**, 449–450.

40. Fujimoto, Y., Ishihara, J., Maki, S., Fujioka, N., Wang, T., Furuta, T. *et al.* (2001). On the bioactive conformation of the rhodopsin chromophore: absolute sense of twist around the 6-*s-cis* bond. *Chem. Eur. J.* **7**, 4198–4204.

41. Fujimoto, Y., Fishkin, N., Pescitelli, G., Decatur, J., Berova, N. & Nakanishi, K. (2002). Solution and biologically relevant conformations of enantiomeric 11-*cis*-locked cyclopropyl retinals. *J. Am. Chem. Soc.* **124**, 7294–7302.

42. Pan, D., Ganim, Z., Kim, J. E., Verhoeven, M. A., Lugtenburg, J. & Mathies, R. A. (2002). Time-resolved resonance Raman analysis of chromophore structural changes in the formation and decay of rhodopsin's BSI intermediate. *J. Am. Chem. Soc.* **124**, 4857–4864.

43. Nevzorov, A. A., Moltke, S., Heyn, M. P. & Brown, M. F. (1999). Solid-state NMR line shapes of uniaxially oriented immobile systems. *J. Am. Chem. Soc.* **121**, 7636–7643.

44. Crozier, P. S., Stevens, M. J., Forrest, L. R. & Woolf, T. B. (2003). Molecular dynamics simulation of dark-adapted rhodopsin in an explicit membrane bilayer: coupling between local retinal and larger scale conformational change. *J. Mol. Biol.* **333**, 493–514.

45. Jäger, F., Jäger, S., Krautle, O., Friedman, N., Sheves, M., Hofmann, K. P. *et al.* (1994). Interactions of the β-ionone ring with the protein in the visual pigment rhodopsin control the activation mechanism. An FTIR and fluorescence study on artificial vertebrate rhodopsins. *Biochemistry*, **33**, 7389–7397.

46. Nakanishi, K. & Crouch, R. (1995). Application of artificial pigments to structure determination and study of photoinduced transformations of retinal proteins. *Isr. J. Chem.* **35**, 253–272.

47. Spooner, P. J. R., Sharples, J. M., Goodall, S. C., Bovee-Geurts, P. H. M., Verhoeven, M. A., Lugtenburg, J. *et al.* (2004). The ring of the rhodopsin chromophore in a hydrophobic activation switch within the binding pocket. *J. Mol. Biol.* **343**, 719–730.

48. Farrens, D. L., Altenbach, C., Yang, K., Hubbell, W. L. & Khorana, H. G. (1996). Requirement of rigid-body motion of transmembrane helices for light activation of rhodopsin. *Science*, **274**, 768–770.

49. Patel, A. B., Crocker, E., Eilers, M., Hirshfeld, A., Sheves, M. & Smith, S. O. (2004). Coupling of retinal isomerization to the activation of rhodopsin. *Proc. Natl Acad. Sci. USA*, **101**, 10048–10053.

50. Kim, J.-M., Altenbach, C., Kono, M., Oprian, D. D., Hubbell, W. L. & Khorana, H. G. (2004). Structural origins of constitutive activation in rhodopsin: role of

the K296/E113 salt bridge. *Proc. Natl Acad. Sci. USA*, **101**, 12508–12513.

51. Harbison, G. S., Smith, S. O., Pardoen, J. A., Courtin, J. M. L., Lutgenburg, J., Herzfeld, J. *et al.* (1985). Solid-state ^{13}C NMR detection of a perturbed 6-s-trans chromophore in bacteriorhodopsin. *Biochemistry*, **24**, 6955–6962.

52. Horiuchi, S., Tokunaga, F. & Yoshizawa, T. (1980). Circular dichroism of cattle rhodopsin and bathorhodopsin at liquid nitrogen temperatures. *Biochim. Biophys. Acta*, **591**, 445–457.

53. Luecke, H. & Lanyi, J. K. (2003). Structural clues to the mechanism of ion pumping in bacteriorhodopsin. *Adv. Protein Chem.* **63**, 111–130.

54. Vogeley, L., Sineshchekov, O. A., Trivedi, V. D., Sasaki, J., Spudich, J. L. & Luecke, H. (2004). *Anabaena* sensory rhodopsin: a photochromic color sensor at 2.0 Å. *Science*, **306**, 1390–1393.

55. Smith, S. O., Palings, I., Copié, V., Raleigh, D. P., Courtin, J., Pardoen, J. A. *et al.* (1987). Low-temperature solid-state ^{13}C NMR studies of the retinal chromophore in rhodopsin. *Biochemistry*, **26**, 1606–1611.

56. Moltke, S., Nevzorov, A. A., Sakai, N., Wallat, I., Job, C., Nakanishi, K. *et al.* (1998). Chromophore orientation in bacteriorhodopsin determined from the angular dependence of deuterium NMR spectra of oriented purple membranes. *Biochemistry*, **37**, 11821–11835.

57. Yoshizawa, T. & Shichida, Y. (1982). Low-temperature circular dichroism of intermediates of rhodopsin. *Methods Enzymol.* **81**, 634–641.

58. Yan, E. C. Y., Kazmi, M. A., Ganim, Z., Hou, J.-M., Pan, D., Chang, B. S. W. *et al.* (2003). Retinal counterion switch in the photoactivation of the G protein-coupled receptor rhodopsin. *Proc. Natl Acad. Sci. USA*, **100**, 9262–9267.

59. Lüdeke, S., Beck, R., Yan, E. C. Y., Sakmar, T. P., Siebert, F. & Vogel, R. (2005). The role of Glu181 in the photoactivation of rhodopsin. *J. Mol. Biol.* **353**, 345–356.

60. Martínez-Mayorga, K., Pitman, M. C., Grossfield, A., Feller, S. E. & Brown, M. F. (2006). Retinal counterion switch mechanism in vision evaluated by molecular simulations. *J. Am. Chem. Soc.* **128**, 16502–16503.

61. Salgado, G. F. J., Struts, A. V., Tanaka, K., Krane, S., Nakanishi, K. & Brown, M. F. (2006). Solid-state ^{2}H NMR structure of retinal in metarhodopsin I. *J. Am. Chem. Soc.* **128**, 11067–11071.

62. Fahmy, K., Jäger, F., Beck, M., Zvyaga, T. A., Sakmar, T. P. & Siebert, F. (1993). Protonation states of membrane-embedded carboxylic acid groups in rhodopsin and metarhodopsin II: a Fourier-transform infrared spectroscopy study of site-directed mutants. *Proc. Natl Acad. Sci. USA*, **90**, 10206–10210.

63. Singh, D., Hudson, B. S., Middleton, C. & Birge, R. R. (2001). Conformation and orientation of the retinyl chromophore in rhodopsin: a critical evaluation of recent NMR data on the basis of theoretical calculations results in a minimum energy structure consistent with all experimental data. *Biochemistry*, **40**, 4201–4204.

64. Creemers, A. F. L., Kiihne, S., Bovee-Geurts, P. H. M., DeGrip, W. J., Lutgenburg, J. & de Groot, H. J. M. (2002). ^{1}H and ^{13}C MAS NMR evidence for pronounced ligand-protein interactions involving the ionone ring of the retinylidene chromophore in rhodopsin. *Proc. Natl Acad. Sci. USA*, **99**, 9101–9106.

65. Seol, Y., Skinner, G. M. & Visscher, K. (2004). Elastic properties of a single-stranded charged homopolymeric ribonucleotide. *Phys. Rev. Letters*, **93**, 118102-1–118102-4.

66. Keller, D., Swigon, D. & Bustamante, C. (2003). Relating single-molecule measurements to thermodynamics. *Biophys. J.* **84**, 733–738.

67. Grossfield, A., Feller, S. E. & Pitman, M. C. (2006). A role for direct interactions in the modulation of rhodopsin by ω-3 polyunsaturated lipids. *Proc. Natl Acad. Sci. USA*, **103**, 4888–4893.

68. MacKerell, A. D., Jr, Bashford, D., Bellott, M., Dunbrack, R. L., Evanseck, J. D., Field, M. J. *et al.* (1998). All-atom empirical potential for molecular modeling and dynamics studies of proteins. *J. Phys. Chem. B*, **102**, 3586–3616.

69. Saam, J., Tajkhorshid, E., Hayashi, S. & Schulten, K. (2002). Molecular dynamics investigation of primary photoinduced events in the activation of rhodopsin. *Biophys. J.* **83**, 3097–3112.

70. Klauda, J. B., Brooks, B. R., MacKerell, A. D., Venable, R. M. & Pastor, R. W. (2005). An ab initio study on the torsional surface of alkanes and its effect on molecular simulations of alkanes and a DPPC bilayer. *J. Phys. Chem. B*, **109**, 5300–5311.

71. Pastor, R. W., Venable, R. M. & Feller, S. E. (2002). Lipid bilayers, NMR relaxation, and computer simulations. *Acc. Chem. Res.* **35**, 438–446.

72. Pitman, M. C., Suits, F., MacKerell, A. D. & Feller, S. E. (2004). Molecular-level organization of saturated and polyunsaturated fatty acids in a phosphatidylcholine bilayer containing cholesterol. *Biochemistry*, **43**, 15318–15328.

73. Brooks, B. R., Bruccoleri, R. E., Olafson, B. D., Swaminathan, S. & Karplus, M. (1983). CHARMM: a program for macromolecular energy, mininization, and dynamics calculations. *J. Comp. Chem.* **4**, 187–217.

74. Fitch, B. G., Germain, R. S., Mendell, M., Pitera, J., Pitman, M., Rayshubskiy, A. *et al.* (2003). Blue Matter, an application framework for molecular simulation on Blue Gene. *J. Para. Distrib. Comp.* **63**, 759–773.

75. Tanizaki, S. & Feig, M. (2005). A generalized Born formalism for heterogeneous dielectric environments: application to the implicit modeling of biological membranes. *J. Chem. Phys.* **122**, 124706-1–124706-13.

76. Tanizaki, S. & Feig, M. (2006). Molecular dynamics simulations of large integral membrane proteins with an implicit membrane model. *J. Phys. Chem. B*, **110**, 548–556.

77. Karplus, M. & Kushick, J. N. (1981). Method for estimating the configurational entropy of macromolecules. *Macromolecules*, **14**, 325–332.

Edited by B. Honig